applied sciences

MDPI

Article

Stick-Slip Phenomena and Acoustic Emission in the Hertzian Linear Contact

Laura Mariana Babici [1,2,*], Andrei Tudor [2] and Jordi Romeu [1]

[1] Acoustical and Mechanical Engineering Laboratory (LEAM), Universitat Politècnica de Catalunya (UPC), c/Colom, 11, 08222 Terrassa, Spain
[2] Department of Machine Elements and Tribology, University POLITEHNICA Bucharest, 313 Splaiul Independentei, 060042 Bucharest, Romania
* Correspondence: laura.mariana.babici@upc.edu; Tel.: +34-937398718

Abstract: AE detection and analysis usually requires a specific, costly platform due to its particular burst nature and high-frequency content. This experimental study investigates the relationship between low-demand acoustic emission parameters (AE) and the occurrence of stick–slip (SS) at the Hertzian linear contact. Hence, the correlation of basic AE characteristics (amplitude, energy, and evolution in time) with stick–slip characteristics (static and kinetic friction coefficients, amplitude, energy, and evolution in time) is pursued. Tribological tests were conducted on cylinder–plane specimens under dry friction conditions with different loads at different low driving speeds and Hertzian contact pressures at a constant stiffness. The AE, normal, and friction forces were recorded simultaneously on the experimental stand. At the cylinder–plane interface, the jumps specific to the stick–slip phenomenon (friction coefficient—COF) were followed after a few milliseconds by AE jump peaks. The results of the experiments show that the amplitude and energy generated by AE were sensitive to the occurrence of the stick–slip phenomenon, while the AE and COF energies in the stick and slip phases had the same law of variation based on the driving velocities. The results show that the amplitude and energy of the sampled low-frequency AE signals were enough to detect the friction in SS and demonstrate the potential of AE as a tool for detecting and monitoring the tribological behaviour of SS at the linear Hertzian contact.

Keywords: stick–slip; acoustic emission; linear Hertzian contact; friction coefficient

Citation: Babici, L.M.; Tudor, A.; Romeu, J. Stick-Slip Phenomena and Acoustic Emission in the Hertzian Linear Contact. *Appl. Sci.* **2022**, *12*, 9527. https://doi.org/10.3390/app12199527

Academic Editor: Giuseppe Lacidogna

Received: 11 August 2022
Accepted: 19 September 2022
Published: 22 September 2022

1. Introduction

The stick–slip phenomenon is characterised as a jerky motion at low and very low driving speeds in a frictional couple. During sliding, this phenomenon occurs if two types of conditions are met—necessary and sufficient. The necessary conditions are given by a decrease in the friction kinetic coefficient with an increase in the driving speed and the dependence of the friction static coefficient on the sticking time. At the same time, the value of the static friction coefficient between two contact surfaces must be greater than the value of the kinetic friction coefficient. A quantitative relationship provides sufficient conditions among the driving speed (order of magnitude from microns/s to mm/s), the moving body mass, and the finite stiffness system in the sliding direction. [1–3].

The theory established by Hertz for the normal non-conforming contact with friction between two bodies with elliptical profiles represents a landmark in linear elasticity [4]. Although the theory of Hertz refers only to elastic contact under normal force or normal force with adhesion, the knowledge of the pressure distribution, the deformations at the connection between two bodies, and the mechanical properties of the materials allow for an extension to a compound analysis with tangential and friction forces generated by sliding or rolling. [5]. Contact friction between solid bodies under sliding conditions gives rise to various waveforms and oscillations within the contact, resulting in sound radiation, including acoustic emission [6].

Acoustic emission refers to transitory mechanical waves in the high-frequency range that are produced by elastic stress energy released in a solid material under mechanical stress. The propagation of elastic waves and oscillations due to the appearance of microcracks, deformations, and fibre breakage in solid bodies are manifested by acoustic emission [7] and can be detected by AE-devoted transducers placed on or near the monitored interface [8].

Initially, in the tribology field, AE has been proposed to monitor the operating condition of bearings [9], cutting tools [10], surface finishing processes [11], sanding [12], and rotary machines [13]. The AE could assess the behaviour of machining tools during operation [14,15]. The AE measurement method is appropriate for discovering initial structural changes in materials. For example, for complex systems, such as the piston–ring–cylinder system of diesel engines, the sources of acoustic emissions are signalled when the engine speed, load, and lubrication conditions change [16]. The active monitoring and diagnosis of various machine components, such as bearings, gears, pumps, and motors, are assessed by AE evaluation over time [17,18]. In addition, the generation of AE at different pressures and sliding speeds has been evaluated by basic methods for rough/finish turning [19,20], detection of the breakdown of a machine tool device [21,22], or in the case of disc brake friction couple components [23].

Regarding the acoustic emission related to the stick–slip phenomena, experimental research has shown the occurrence of AE during the sliding and rubbing of flat surfaces of various materials, such as rock [24], granite [25], and composite materials [26]. Studies on the stick–slip phenomenon in O-ring sealing samples [27] and the contact between a mild steel sample and hardened steel clamps [28] have shown the importance of AE utility in tribology.

The origin of acoustic emission is the internal modifications in the materials due to an external stimulus. These modifications are usually composed of discrete events so that the emission of elastic waves is in the form of bursts or pulses of distinctive characteristics. Therefore, the analysis of signals captured in the AE test is usually performed considering this discrete nature, using a rather complex range of parameters related to the wave pulses, such as the number of counts, the rise and disappearance time, or frequency content-related variables [29–33]. This analytical strategy, combined with the frequency content, typically in the ultrasound range (>20 kHz), leads to the need for specific equipment, both hardware and software, to carry out these very specific tests. However, some less demanding parameters, such as the power of the square signal integrated over the signal period (AErms), have been successfully used to quantify pseudo-continuous emissions [34,35], even in wear and friction phenomena [36–38].

The present work aimed to use parameters of the AE signal with low hardware and software demand, i.e., those that can be calculated from a signal captured by a multipurpose data acquisition system for mechanical tests, to detect the occurrence of the stick–slip phenomenon at the Hertzian linear contact in dry friction conditions.

In addition, the analysis of the correlation between the stick–slip amplitude and the amplitude of the acoustic emission provides a new quantitative identification of tribological states in different conditions of contact pressures and very low driving speeds. The energy generated by AE and the energy consumed by friction for stick and slip phases were determined and analysed based on the Pearson correlation coefficient, while the correlation of these energies as a function of the driving and sliding speeds were obtained from the logarithmic fitting. With this, the AE accompanies the friction process and becomes, for Hertzian linear contact, a non-destructive tool for detecting and monitoring the stick–slip phenomenon.

2. Experimental Model—Geometry and Material of Specimens

The flat specimen was made of unhardened and unalloyed steel, type R260 (EN 13674-1:2018) with a Brinell hardness of 285 HBW, and the cylinder specimen was made of surface-treated steel, type ER7 (EN 13262:2021) with a Brinell hardness of 265 HBW.

These wear-resistant materials are used for the rails and wheels in railway systems. The surface quality of the specimens was initially evaluated by measuring the roughness with a Gaussian filter of 0.8 mm in the longitudinal (L) and transverse (T) directions with Surtronic 25 equipment. Thus, the average roughness values of the cylinder specimen were 0.734 µm (L) and 2.15 µm (T), and for the flat specimen, 1.13 µm (L) and 1.17 µm (T). The sizes of the cylinder and flat samples are shown in Figure 1. The fixing drawbar of the cylindrical specimen was incorporated into the tribometer loading device. Applying a known tangential force on its free end caused bending of the drawbar–cylinder system, which could be measured, and thus, the sample stiffness was obtained (straight slope—30.427 N/mm). This stiffness influences the amplitude of the stick–slip phenomenon; hence, the greater the stiffness, the more the stick–slip phenomenon will decrease until it disappears. Although the effect of the frictional force on deformation is essential, frictional force does not depend on stiffness.

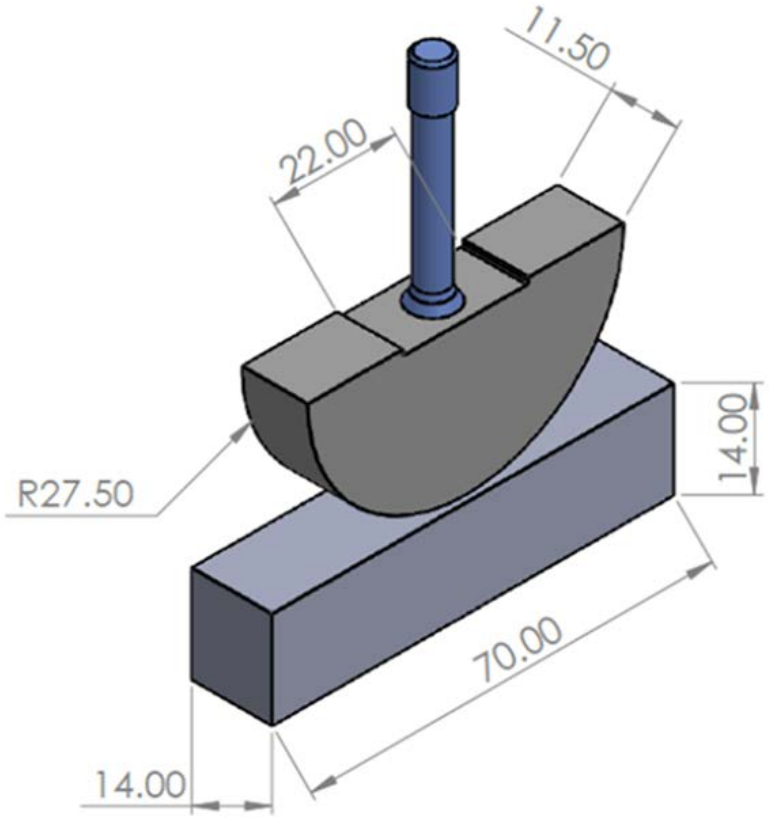

Figure 1. Dimensions for cylindrical and plane specimens used for tests.

The cylindrical sample moved vertically until it arrived at the flat specimen under predetermined conditions. In this position, it was loaded at a normal force (F_n = 20, 40, 60 N). The flat test piece moved linearly on a horizontal plane with a driving speed, thus achieving the frictional force. This device simulated linear contact with tangential and normal forces at very low sliding speeds, specific to contact with forced rolling. The device allowed for the experimental detection of one of the effects of rolling motion micro slips, namely the dynamics of sliding friction at low speeds and contact pressures with elliptical Hertz type distribution. This distribution led to a flat surface of the elastically deformed bodies, whilst the friction force between the specimens depended on the evolution of the friction coefficients with the driving speed (v) and sliding speed (v_{slip}).

The experimental setup presented in this paper was carried out in CERT UMT-2 Tribometer, which is used to test the stick–slip phenomenon of different materials. Figure 2 shows the test system with the upper and lower specimens connected to the tribometer. The tribometer was adapted to the specific slip conditions for Hertzian linear contact to perform these experimental tests. Thus, the clamping systems of the lower flat sample and

the cylindrical sample with the bending stiffness calibrated to detect the SS phenomenon were designed and made for these experimental tests. The tribometer was equipped with a two-dimensional force sensor DFH-20 that was used to measure the control of a normal loading force and friction force between the upper and lower test pieces. The damping system, located between the force sensor and the upper sample support, was used to maintain a constant load force during the tests. In order to maintain the normal force as constantly as possible at the contact of the samples, the tribometer was equipped with a device with a spring and shock absorber that allowed for the continuous adjustment of the normal force depending on the "response" of the material of the flat sample. The upper specimen was plugged into the monitoring system, while the lower specimen was connected to the L20HE linear motion unit.

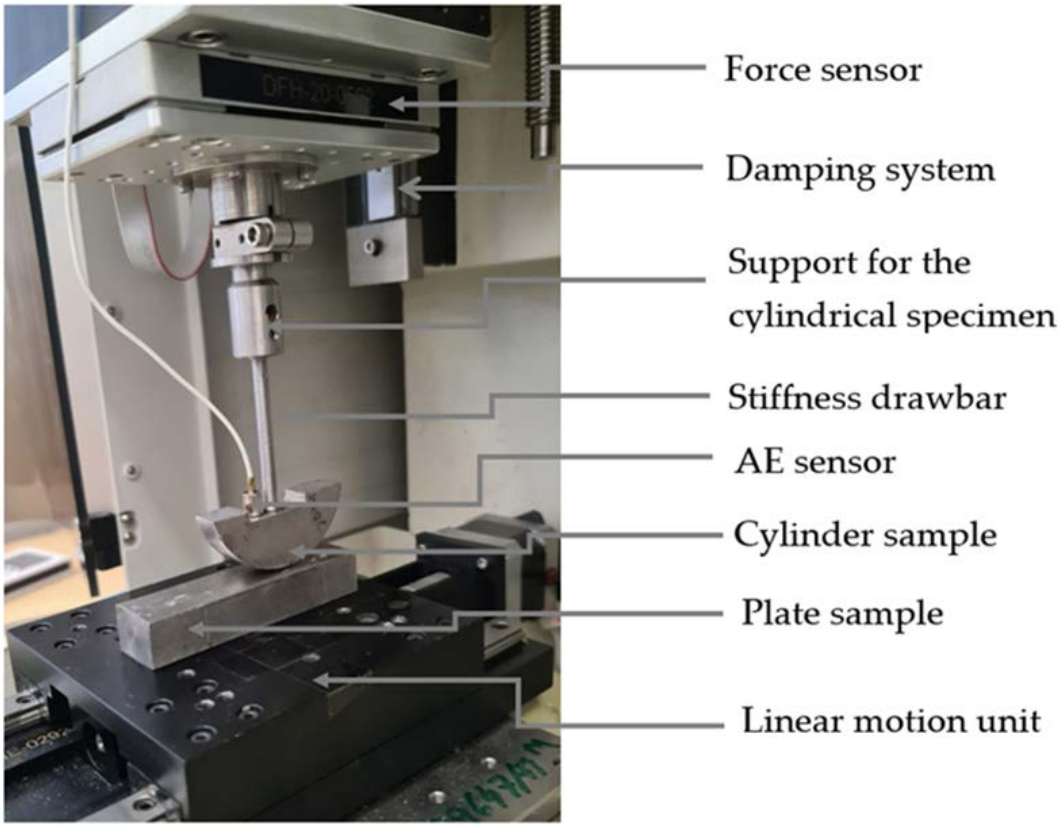

Figure 2. Tribometer to study the phenomenon of stick–slip.

The adhesion at the molecular level and the elastic–plastic deformations at the roughness level are both responsible for friction, which in turn is responsible for tangential force [39–41]. A CETR AE-5 AE sensor with a frequency range between 0.2 MHz and 5 MHz, integrated with the UMT-2 tribometer, was intended to measure the acoustic emission signals during the friction test. It was mounted on the side of the cylinder specimen. The AE signal, along with those related to force and position, was acquired by the CETR UMT control unit at a 200 kHz sampling rate. The AE signal was amplified with a gain of 60 dB, and its RMS value was calculated every 0.5 s.

The primary purpose of the experimental tests presented was to determine the evolution of the static and kinetic friction coefficients of the stick–slip phenomenon accompanied by the appearance of the acoustic emission at the Hertzian linear contact. The beginning of friction is a fundamental and essential issue in understanding the principle of tribology, an effect observed for different sliding speeds, three contact forces, and three contact pressures.

3. Methodology

One goal of this study was to demonstrate that the basic parameters of the AE are suitable and sufficient to detect the SS phenomenon and, thus, the adapted configuration of the Tribometer UMT-2 prepared for this type of experiment led to a simplified but sufficient analysis of the AE signals, avoiding the requirements of standard AE equipment. Moreover, the fundamental objective of the experimental tests carried out was to analyse the correlations of the AE and COF parameters, depending on the low and very low driving speeds, because the initiation of the relative motion between two bodies under friction is a fundamental and essential problem in understanding the friction principle in tribology.

The tribometer was equipped with tensometric transducers for normal and tangential stresses and AE and driving speed transducers. Due to the calibration of the bending stiffness on the vertical drawbar that was mounted on the cylindrical specimen (the bending deformation occurred depending on the force applied perpendicularly to the drawbar), the tangential force was determined as a frictional force. The driving speed was determined by adjusting the time and distance. The synchronization of the friction force measurement with the AE measurement was automatic. Based on the friction force, the normal force and AE were measured directly by the transducers and could be determined indirectly by calculating the average of each COF (static, kinetic, amplitude), sliding speed, energy consumed by friction, and several AE parameters (counts, amplitude, energy).

Before starting the tests, at the lowest normal load and driving speed, five assays were performed in order to "adapt" the surfaces to each other, and then the tests were run from the highest to the lowest driving speed with progressively increasing normal force. In order to analyse the phenomenon of stick–slip, 12 tests were performed. For these, four driving speeds (0.2, 0.1, 0.05, and 0.01 mm/s), four time periods (50, 100, 200, and 1000 s), and three normal load forces (20, 40, and 60 N) were set [42], resulting in three Hertzian contact pressures (48.20, 68.16, and 83.48 MPa), determined by calculation. Each test result was obtained from an average of three identical attempts performed under the same conditions (the normal loads and driving speeds applied), and the coefficient of statistical variation was determined as the ratio between the mean square deviation and the arithmetic mean. The highest value of the statistical coefficient of variation for all tests (three forces and four speeds) was 0.08. The stick–slip periods used in the investigation were chosen from the stabilised zone of the movement, taken into account after two or three jumps from the initiation of the movement.

The stick and slip periods were analysed, and for each jump sequence between static and kinetic friction, the static friction coefficients μ_s, the kinetic friction coefficients μ_k, and the amplitude of the stick–slip phenomenon μ_v were determined, where $\mu_v = (\mu_s - \mu_k)/2$. The maximum static friction coefficient is the peak of the phenomenon, and the kinetic one is the minimum. These coefficients are approximately constant at the same load and speed (the COF is considered a deterministic phenomenon).

For each normal force and speed, the peaks of the static friction coefficients were counted (the static friction coefficient number is equal to the kinetic friction coefficient number), resulting in a frequency of stick–slip jumps relative to the period time.

In this work, the count of AE refers to all AE peaks above the threshold value (set to 0.02 V). Only the signals that exceeded the voltage threshold are identified as AE signals. For each stick and slip phase sequence in a test, each AE count was obtained over time, and finally, the average peak results were obtained for each test.

The AE amplitude, directly connected to the AE energy, denotes the highest measured voltage in a waveform. The energy induced in the system by friction (W_{COFst} and W_{COFsl}) during the stick–slip period is the integral defined by the friction force ($F_f = F_n$ COF) and the length of the friction path ($L_f = v \cdot t$). In the stick phase, there is no movement between the specimens, but the static friction force deforms elastically, and the system accumulates energy.

The energy generated by the acoustic emission (W_{AEst} and W_{AEsl}) during the stick–slip period is defined as the integral (area) of the square voltage (V_{AE}) emitted over time.

The instantaneous speed in the slip phase is defined as the derivative of the distance covered by the cylindrical specimen during the slip time. This distance was determined by the lower test piece moving at a fixed translation speed (driving). The average slip speed was obtained from reporting the distance covered by the upper specimen in the slip phase (determined by the jump between the static friction force characteristic of the tip and the minimum kinetic friction force and the known system rigidity) during the slip phase. This time was determined from the recording of the phenomenon.

Error bars are graphical representations of data variability that are used on graphs to show the error or uncertainty in a given measurement; however, error bars frequently reflect one standard error, a standard deviation of uncertainty, or a certain confidence interval (e.g., a 95% interval). The Pearson correlation coefficient was used to determine the correlations between the COF and AE amplitudes, as well as the energies between them, whose values higher than 0.75 indicate a high correlation between these parameters. The results of the *p* test show the percentages of the confidence levels of the results obtained [43–45].

4. Results and Discussion

The friction coefficient evolution accompanied by AE is presented as an example of the results obtained for the driving speed of 0.01 mm/s at normal forces of 20–60 N. (Figure 3a–c) and the friction coefficient evolution for the force of 60 N at the four driving speeds (Figure 3d). In all cases, the presence of the stick–slip phenomenon was confirmed by COF variation. In general terms, the stick–slip jumps coincided with the sudden increases in AE, although for a 20 N load, this coincidence was not always present.

As a general trend, a high normal load and slow driving speed tended to create a stick–slip phenomenon of low frequency and high amplitude, as shown in Table 1, where each value represents an average of all stick–slip events at a specific normal force and driving speed (the same holds for all figures). The driving speed, sliding speed, and normal load are the major factors that play a significant role in the variation of friction coefficients [46–48]. The driving speed and normal load are directly measured from tests, and the sliding speed is easily calculated from the time and displacement of each phase. The sliding speed is related to the stick–slip frequency and amplitude; therefore, a higher normal load and slower driving speed tended to increase the sliding speed due to the stick–slip phenomena of low frequency and high amplitude (Figure 4).

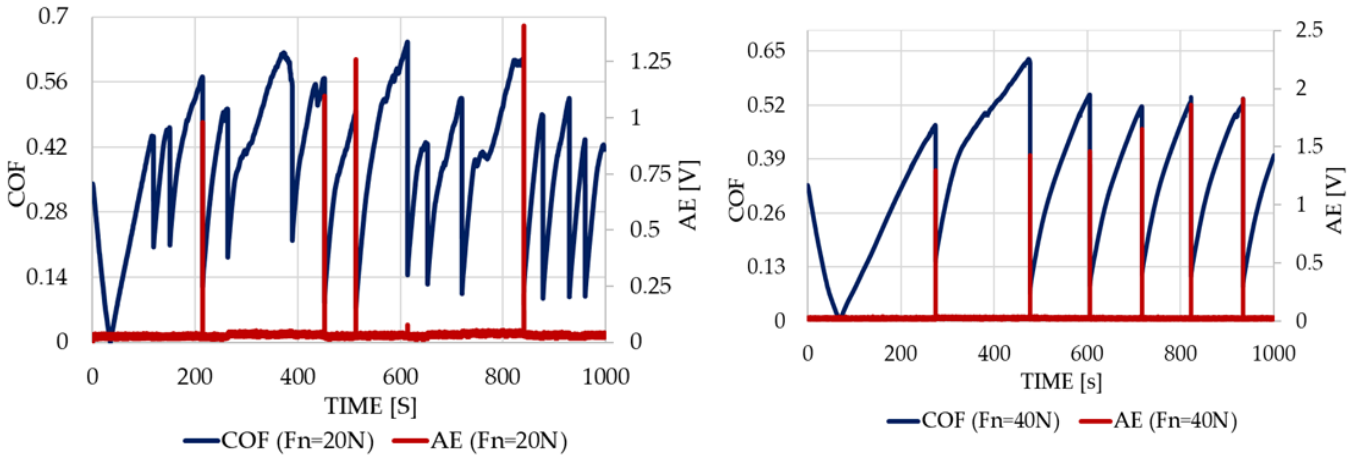

(**a**) (**b**)

Figure 3. *Cont.*

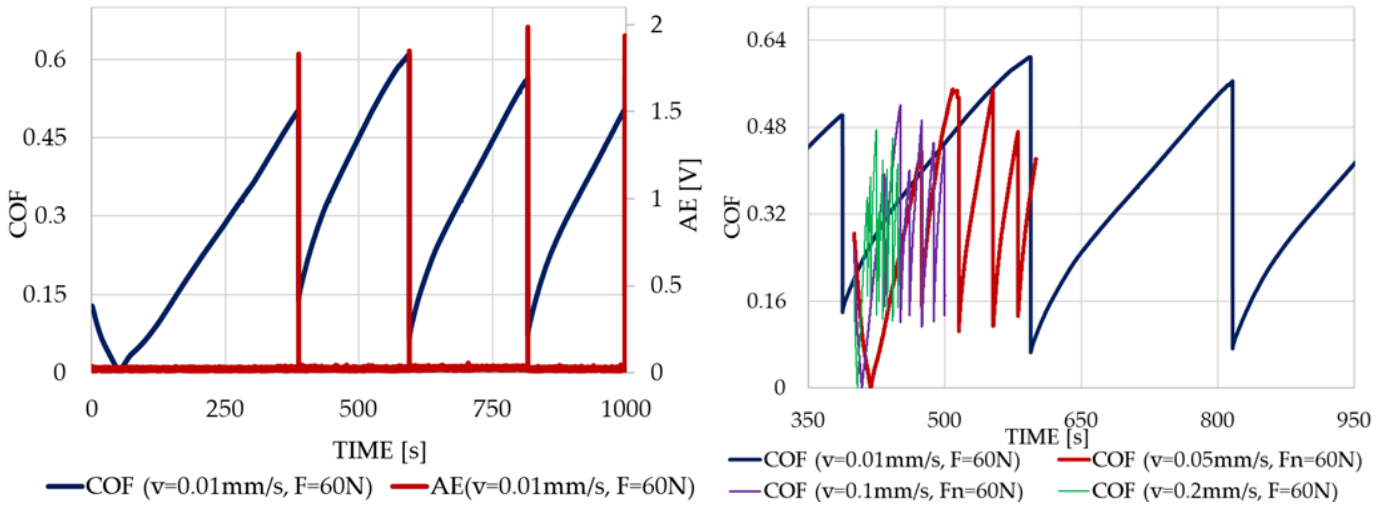

(**c**) (**d**)

Figure 3. COF and AE amplitude with a driving speed of 0.01 mm/s for the normal force of 20 N (**a**), 40 N (**b**), and 60 N (**c**). Comparison of COF results over time at 60 N force and all driving speeds (**d**).

Table 1. Values of the friction coefficients.

Sliding Speed (mm/s)	F_n = 20 N			F_n = 40 N			F_n = 60 N		
	μ_{s1} *	μ_{k1} **	μ_{v1} ***	μ_{s2} *	μ_{k2} **	μ_{v2} ***	μ_{s3} *	μ_{k3} **	μ_{v3} ***
0.2	0.304	0.224	0.040	0.386	0.180	0.103	0.417	0.162	0.128
0.1	0.383	0.239	0.072	0.418	0.186	0.116	0.429	0.168	0.140
0.05	0.461	0.246	0.108	0.47	0.189	0.141	0.485	0.175	0.155
0.01	0.525	0.282	0.122	0.557	0.262	0.148	0.582	0.250	0.166

* Static friction coefficients. ** Kinetic friction coefficients. *** Amplitude of the stick–slip phenomenon.

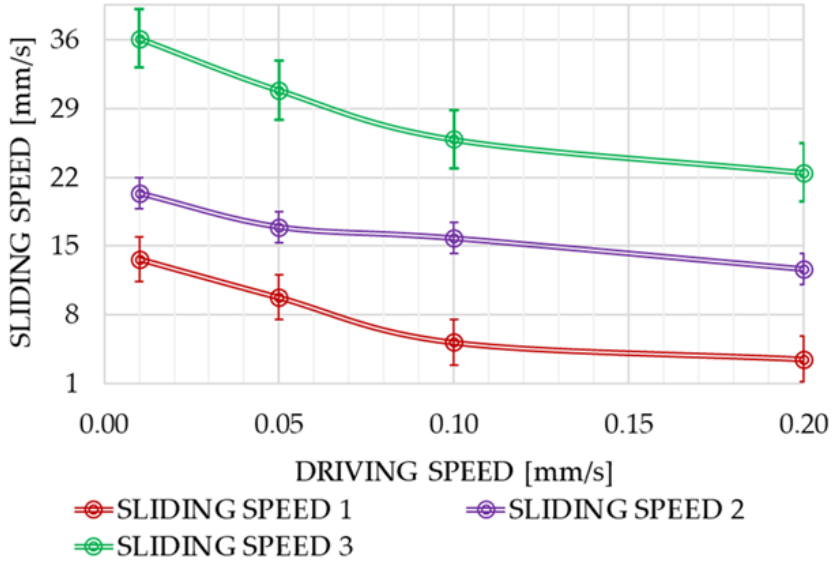

Figure 4. Variation in sliding speed with driving speeds (mm/s), including error bar.

Figure 5 shows the static and kinetic friction coefficients and the stick–slip amplitude for different driving speeds. As expected, the static and kinetic friction coefficients decreased as the driving speed increased to a specific stiffness. Both friction coefficients increased with the soldering time due to the phenomenon of "saturation" of the real contact

area, so the higher the driving speed, the shorter the soldering time and the lower the static and kinetic coefficients [49,50]. The increase in driving speed also reduced the contact surface and, accordingly, the friction coefficient tended to decrease, giving, as a result, a stick–slip movement of lower amplitude (measured by the difference between the static and kinetic COFs), as can be seen in Figure 5c, and higher frequency, as shown in Figure 5d.

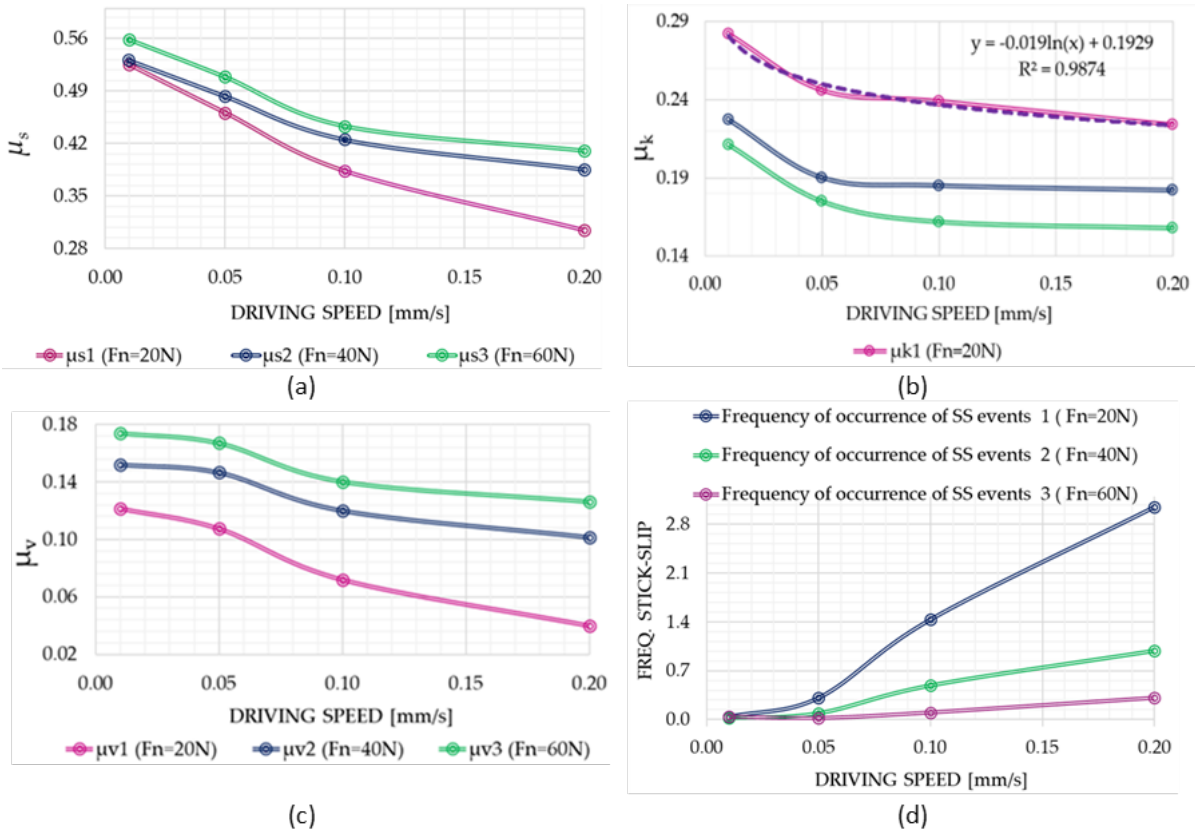

Figure 5. The influence of the driving speed and normal force on the friction coefficients: static friction coefficient (**a**), kinetic friction coefficient, including the fitted curve of the kinetic friction coefficient with a force of 20 N (**b**), the amplitude of the stick–slip phenomenon (**c**) with the frequency of the number of the stick–slip jumps (**d**).

Further increases in the driving speed would lead to the possible cancellation of the stick–slip phenomenon. The effect of the normal load is the increase in the static coefficient of the friction force because the contact pressure and real contact area also increase. In addition, according to the known molecular–mechanical [51,52] friction theory for conventional dry contact, the kinetic friction coefficient decreases with a decreasing normal force. This divergence in the static and kinetic friction behaviour regarding the normal load leads to a stick–slip movement of a lower frequency and higher amplitude.

In addition, Figure 5b shows the dependence between the kinetic friction coefficients on the driving speed, which decrease with increases in the driving speed of the surface, approximated by the logarithmic curves of the form y = a + (b ln (x)) as has been previously found by Helstot and Caroli [53,54].

The Pearson correlation coefficients were calculated between the amplitude of the SS (μ_v) as an independent variable and the normal force (F_n) and driving speed (v) as dependent variables. The obtained results can be found in Table 2.

Table 2. Correlation between SS amplitude and normal force, respectively, and driving speed.

Coefficients	μ_v/F_n v = 0.2 mm/s	μ_v/F_n v = 0.1 mm/s	μ_v/F_n v = 0.05 mm/s	μ_v/F_n v = 0.01 mm/s
Pearson correlation	0.969 *	0.986 **	0.976 **	0.995 **
Coefficients	μ_v/v F_n = 20 N	μ_v/v F_n = 40 N	μ_v/v F_n = 60 N	
Pearson correlation	−0.986 **	−0.962 *	−0.976 **	

* Correlation is significant at the p = 0.05 level (95% level of confidence). ** Correlation is significant at the p = 0.01 level (98% level of confidence).

Regarding the acoustic emission, as a general trend, there was the continuous activity of low AE in the stick phase; however, there was a burst emission of high amplitude in the sliding phase, and both were dependent on the normal load.

It is easy to see that the AE peaks appeared only at the jumps from the stick to the slip (the transition from static friction to kinetic friction), although they took place with a delay of a few milliseconds compared to the COF. This delay of the AE could be explained by the finite propagation speed of the AE elastic waves compared to the moment of the initiation of the slip phase (Figure 6).

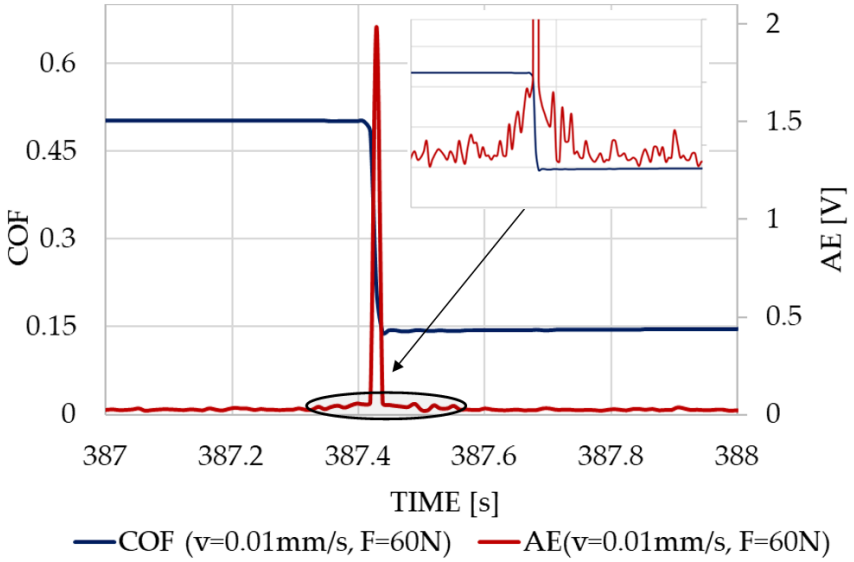

Figure 6. The variation in the friction coefficient and acoustic emission (peak extracted).

In the following, some characteristics of the AE, such as the AE amplitude, AE burst/continuous counts, and AE energy, are analysed in comparison to the characteristics of the stick–slip movement with the aim of investigating if they can be helpful for a comprehensive view of the identification of the stick–slip phenomenon by AE. The counts of AE in the stick and slip phases are presented in Figure 7.

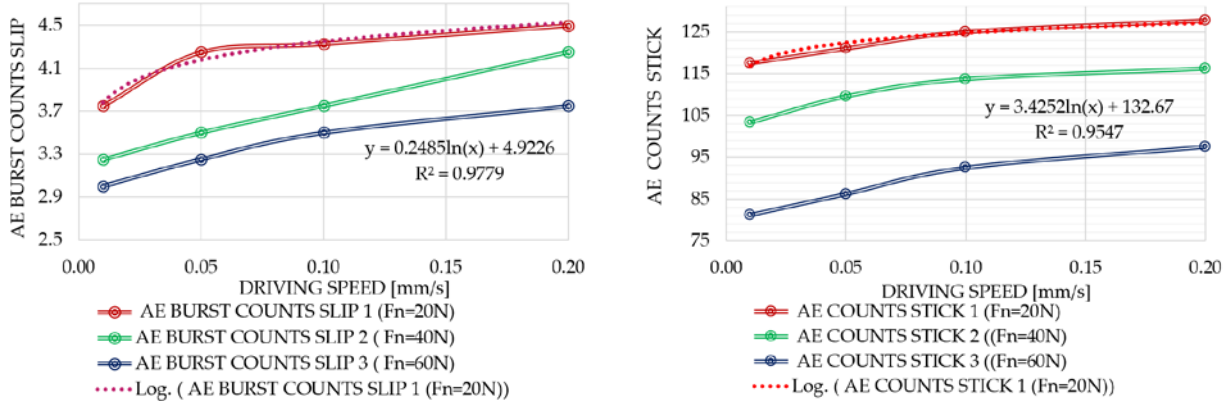

(a) (b)

Figure 7. AE counts in the slip (**a**) and stick (**b**) phases, including the fitted curves of the counts of AE with a force of 20 N.

In both the stick and slip phases, the counts of AE increased with the driving speed and decreases in the normal load. In fact, the higher the frequency of the stick–slip movement, the higher the AE counts. The reason for this result is due to the higher number of stick–slip movements for a single test and because the AE takes place basically at the beginning of the slip movement, as shown in Figure 8. For each slip phase sequence in a test, each AE count was calculated over the slip time, and finally, mediated for each test. Likewise, for the stick phase, the AE counts were determined for each sequence over the stick time, and finally, an average was determined for each test. Therefore, a low frequency, higher amplitude slip-stick movement gives a relatively low count of AE with the burst aspect, mainly occurring at the beginning of the slip movement. However, the fact that some of the bursts are missing due to the low sampling frequency used in this work must be taken into account in consideration of the results related to the counts.

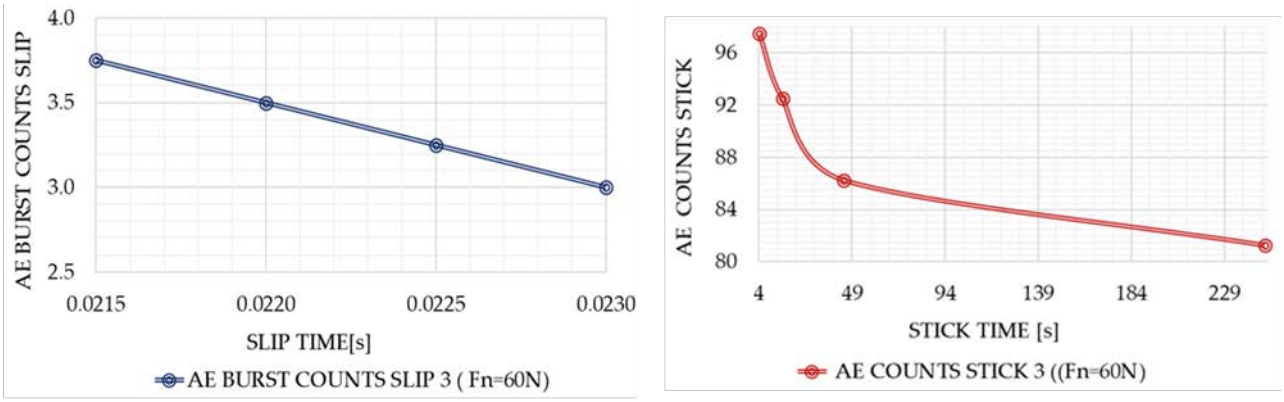

(a) (b)

Figure 8. Distribution of the AE burst counts along the slip time (**a**), and AE counts along the stick time (**b**).

The amplitudes of the AE signal were plotted against driving speed for different loads (Figure 9). In general terms, the AE amplitudes for both the stick and slip phenomena seem to be rather related to the kind of stick–slip movement: the increase in the normal force and the decrease in driving speed led to an increase in the stick–slip movement amplitude, with a consequent rise in the amplitude of the AE bursts. In addition, the amplitude in the stick phase was significantly lower than the amplitude in the sliding phase (Figure 9a, b), as was expected, since the AE caused during the stick phase was only prompted by the

contact surface deformation, while for the slip phase, other phenomena, such as a part of the plastic deformation occurred. In the process of transmitting normal forces between the two bodies and in the presence of relative motion, the "third body" was formed with properties specific to the material couple. Thus, the structure of the material changed, the existing microcracks joined, and new cracks appeared, especially during the appearance of plastic deformations (Figure 9). It was also observed that the AE amplitude follows a logarithmic curve, similar to the friction coefficients, depending on the movement speed.

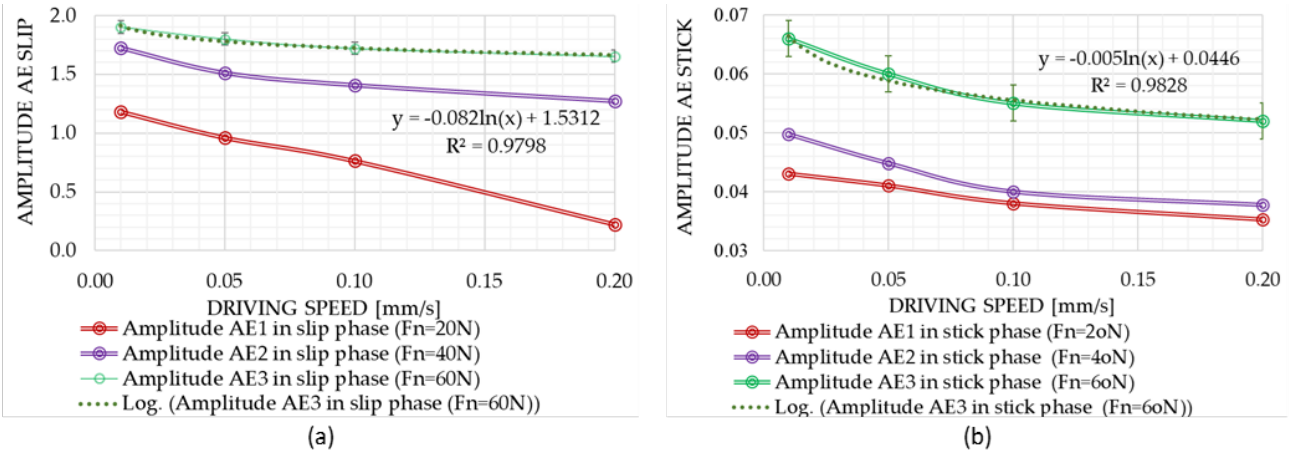

Figure 9. Variation in AE amplitude with driving speed in slip phase (**a**) and stick phase (**b**).

The Pearson correlation coefficients were calculated between the amplitude of the acoustic emission, A_{AEsl} and A_{AEst} from the slip and stick phases, respectively, as an independent variable and the amplitude of the stick–slip phenomenon(μ_v) as a dependent variable. The obtained results can be found in Table 3.

Table 3. Correlations between the AE and stick–slip amplitudes.

Coefficients	A_{AEsl}/μ_v	A_{AEst}/μ_v
	F_n = 20 N	
Pearson correlation	0.980 **	0.997 **
	F_n = 40 N	
Pearson correlation	0.930 *	0.96 *
	F_n = 60 N	
Pearson correlation	0.961 **	0.970 **

* Correlation is significant at the p = 0.05 level (95% level of confidence). ** Correlation is significant at the p = 0.01 level (98% level of confidence).

The Pearson coefficients fall within the 95% confidence interval ($p < 0.05$), and it can be seen that there was a very high correlation between the AE amplitude and the amplitude of the stick–slip phenomena. Considering the high value of the correlation coefficients, we can conclude that the appearance of the stick–slip phenomenon can be identified by determining the amplitude of the acoustic emission.

Knowing that the amplitude of AE is correlated to the amplitude of the stick–slip movement, and the number of counts seems to be rather independent of the amplitude of the movement, it seems that the energy consumed by friction (W_{COF}) and the AE (W_{AE}) energy could also be related. The energy consumed by friction (W_{COF}) and the AE (W_{AE}) energy were calculated for the three forces, 20, 40, and 60 N, and for each phase of soldering and sliding (Figure 10). In general terms, the higher the amplitude of the stick–slip movement, the higher the energy consumed by friction (W_{COF}) due to increases

in the friction force and sliding distance, and the higher energy generated by AE, due to the intensity of the deformation mechanisms in the contact zone.

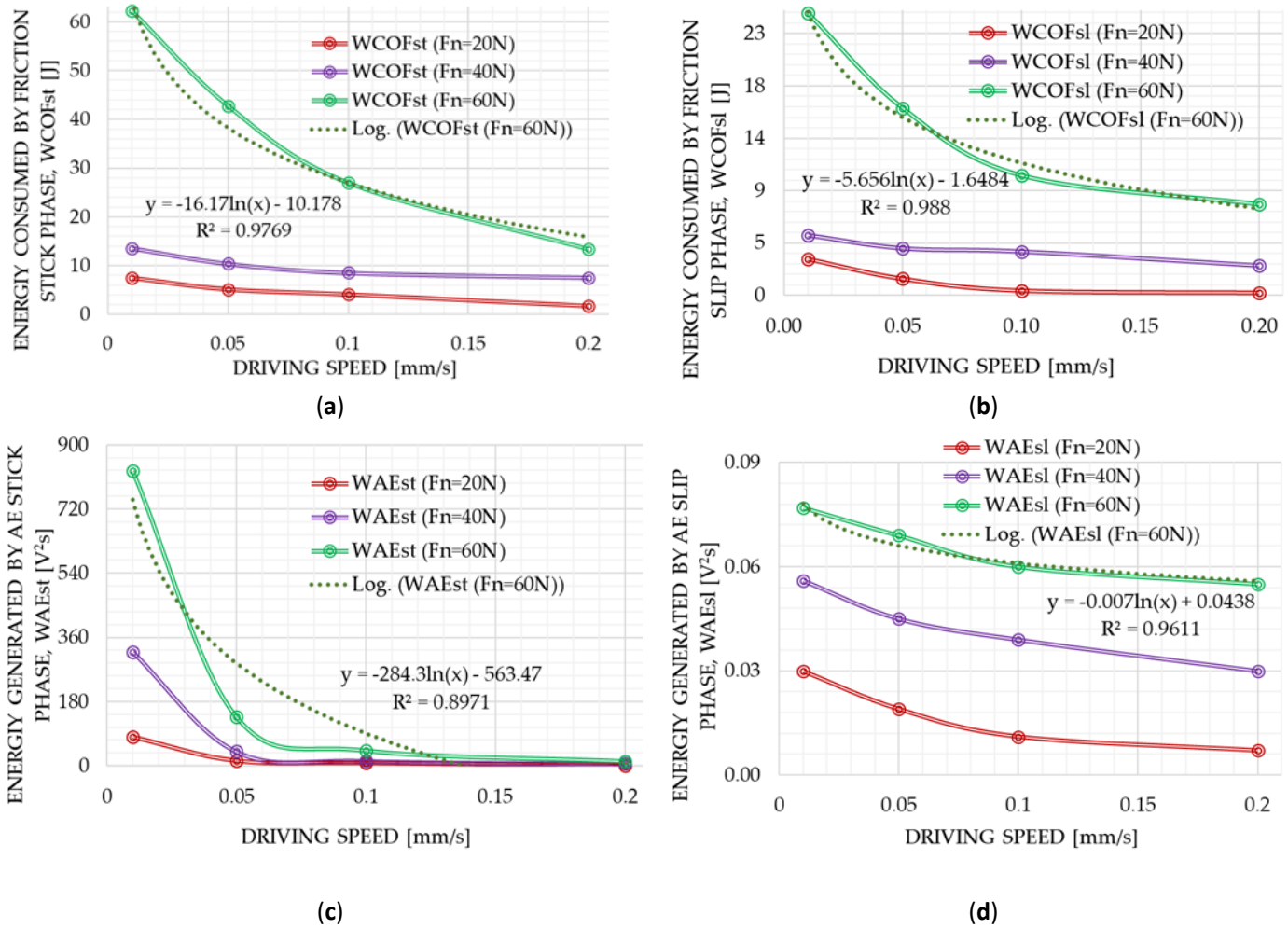

Figure 10. Variation in energies with different driving speeds (mm/s): (**a**) energy consumed by friction in slip phase, W_{COFsl} (J), (**b**) energy consumed by friction in stick phase, W_{COFst} (J), (**c**) energy generated by AE in slip phase, W_{AEsl} (V^2s), (**d**) energy generated by AE in stick phase, W_{AEst} (V^2s).

Therefore, the energies seem to be related to each other and also to the amplitude of the stick–slip movement. The Pearson correlation coefficients were calculated between the energy generated by the acoustic emission, W_{AEsl} (slip), W_{AEst} (stick) and the energy consumed by friction, W_{COFsl} (slip) W_{COFst} (stick), between the SS amplitude (μ_v) and these energies as well as between the AE_{sl} and SS amplitudes and the sliding speed (v_{slip}) (Table 4). Therefore, the energies appear to be related between themselves and also associated with the amplitude of the stick–slip motion. There was always a good correlation between both energies, with slightly reduced results in the stick phase when the 20 N force was applied. There was not always a burst of AE for the slide phase at this low normal force, so the correlation was not as good as for a greater normal load. In addition, at low normal forces, the deformations at the contact level were small; therefore, reduced tangential force effects caused a reduced AE signal.

Table 4. Correlations between the AE and COF energies, stick–slip amplitudes and sliding speed in the stick and slip phases.

Coefficients	W_{AEsl}/W_{COFsl}	W_{AEst}/W_{COFst}	A_{AEsl}/v_{slip}	μ_v/v_{slip}	μ_v/W_{COFsl}	μ_v/W_{COFst}	μ_v/W_{AEsl}	μ_v/W_{AEst}
				F_n = 20 N				
Pearson correlation	0.990 **	0.900 *	0.91 *	0.960 **	0.91 *	0.964 **	0.939 **	0.770 *
				F_n = 40 N				
Pearson correlation	0.991 **	0.934 **	0.963 **	0.937 **	0.921 *	0.91 *	0.945 **	0.72 *
				F_n = 60 N				
Pearson correlation	0.989 **	0.932 **	0.999 **	0.970 **	0.935 *	0.966 **	0.976 **	0.755 *

* Correlation is significant at the p = 0.05 level (95% level of confidence). ** Correlation is significant at the p = 0.01 level (98% level of confidence).

Considering the high value of the correlation coefficients, it seems that the magnitude of the stick–slip phenomenon can be estimated by calculating the energies generated by the acoustic emission, both in the stick phase and the slip phase. The Pearson correlations between the stick–slip amplitude and the COF and AE energies in the stick and slip phases show a close correlation between them (Table 4). The amplitude of stick–slip movement correlates well with the AE energy for the slip phase and not so well (as expected) with the AE energy for the stick phase, but the energy seems not to be as good an indicator of the stick–slip movement amplitude as it is the amplitude of AE. In the stick phase, it is possible that the local elastic deformations were the majority compared to the plastic ones, and as such, the AE energy was reduced. The system (drawbar and cylindrical specimen) was deformed exclusively elastically. The real contact area also contained roughnesses that deformed plastically. There was also a strong positive correlation between the AE and SS amplitudes with the sliding speed for all applied forces (Table 4).

In order to ascertain the origin of the AE, the W_{AE} and W_{COF} in the slip phase were plotted against the sliding speed in Figure 11. The sliding speed is a direct indicator of the amplitude of the stick–slip movement, and, as expected, the friction energy tended to increase with the sliding speed, and it was dependent on the normal force. In addition, the AE energy tended to grow with the sliding speed as well, but it shows some dependence on the normal force, suggesting that other complex phenomena took place at the contact point zone, such as a reduction in tangential stresses and an increase in the contact area.

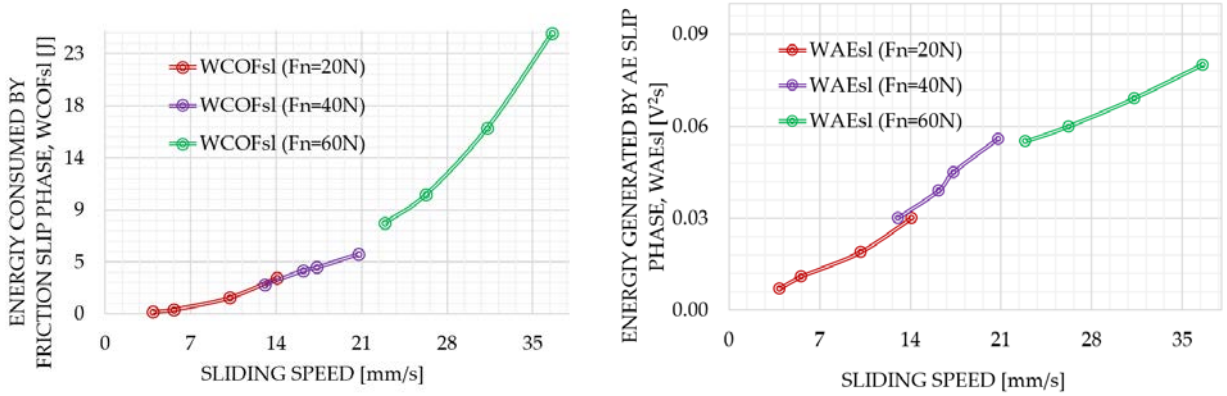

Figure 11. Variation in COF (**a**) and AE (**b**) energies with sliding speed.

5. Conclusions

The acoustic emission signals generated during the relative motion between the cylinder–plane specimens were captured by a multipurpose acquisition system and processed using basic parameters based on the RMS signal in order to determine if the stick–slip appearance and their sensitivity to the onset of movement can be detected and predicted by the acquisition and analysis of the AE using hardware and software with low demand. The tests were conducted under various situations involving normal loads, driving, and sliding velocities. Although the tests were not exhaustive, they verified the feasibility of using non-complex AE parameters as a non-destructive method of detecting the stick–slip phenomenon.

In all tests performed, the presence of the stick–slip phenomenon was confirmed by the COF variation and the coincidence with the bursts of AE for all contact pressures and driving and sliding speeds. The variables that significantly affected the changes in friction coefficients were the driving speed, sliding speed, and normal load. Higher normal loads and slower displacement speeds increased the slip velocity because of the low-frequency, high-amplitude stick–slip phenomena that occurred mostly at the start of the slide movement.

AE is related to this type of motion. In terms of acoustic emission, the stick phase had low AE activity, while the sliding phase exhibited bursts of high amplitude activity that were reliant on the normal load. Jumps from static to kinetic friction (COF) were followed at short time intervals (milliseconds) by acoustic emission (AE) jumps.

The presence of the stick–slip phenomenon can be detected by measuring the amplitude and energies of the acoustic emission revealed by a high positive Pearson correlation between them. The energy consumed by friction (W_{COF}) increased with the amplitude of the stick–slip motion, and the energy generated by AE increased also.

The amplitude and energies generated by the acoustic emission are relevant and confirm the direct dependence on the stick–slip phenomena for the non-lubricated Hertzian linear contact, while the count of AE bursts is not applicable to identifying the magnitude of the stick–slip movement, probably due to the same amount of real bursts missing caused by the relatively low sampling frequency used in this work.

Hence, the acoustic emission detected by analysing the parameters that can be used from a signal captured from a multifunctional platform becomes an essential indicator for detecting and monitoring the stick–slip phenomenon.

Author Contributions: Conceptualisation, L.M.B., A.T. and J.R.; methodology, L.M.B., A.T. and J.R.; software, L.M.B.; validation, L.M.B.; formal analysis, L.M.B., A.T. and J.R.; investigation, L.M.B., A.T. and J.R.; resources, L.M.B., A.T. and J.R.; data curation, L.M.B., A.T. and J.R.; writing—original draft preparation, L.M.B.; writing—review and editing, A.T. and J.R.; visualisation, L.M.B.; supervision, A.T. and J.R. All authors have read and agreed to the published version of the manuscript.

Funding: This research received no external funding.

Institutional Review Board Statement: Not applicable.

Informed Consent Statement: Not applicable.

Data Availability Statement: Not applicable.

Conflicts of Interest: The authors declare no conflict of interest.

References

1. Antoniou, S.S.; Cameron, A.; Gentle, C.R. The friction-speed relation from stick-slip data. *Wear* **1976**, *36*, 235–254. [CrossRef]
2. Bo, L.C.; Pavelescu, D. The friction-speed relation and its influence on the critical velocity of stick-slip motion. *Wear* **1982**, *82*, 277–289.
3. Kato, S.; Sato, N.; Matsubyashi, T. Some Considerations on Characteristics of Static Friction of Machine Tool Slideway. *J. Lubr. Technol.* **1972**, *72*, 234–247. [CrossRef]
4. Storåkers, B.; Elaguine, D. Hertz contact at finite friction and arbitrary profiles. *J. Mech. Phys. Solids* **2005**, *53*, 1422–1447. [CrossRef]
5. Ciavarella, M. Transition from stick to slip in Hertzian contact with "Griffith" friction: The Cattaneo–Mindlin problem revisited. *J. Mech. Phys. Solids* **2015**, *84*, 313–324. [CrossRef]

6. Akay, A. Acoustics of friction. *J. Acoust. Soc. Am.* **2002**, *111*, 1525–1548. [CrossRef]
7. Green, R.E., Jr. Basic Wave Analysis of Acoustic Emission. In *Mechanics of Nondestructive Testing*; Springer: Boston, MA, USA, 1980; pp. 55–76.
8. Dobrynin, S.A.; Kolubaev, E.A.; Smolin, A.Y.; Dmitriev, A.I.; Psakhie, S.G. Time-frequency analysis of acoustic signals in the audio-frequency range generated during Hadfield's steel friction. *Tech. Phys. Lett.* **2010**, *36*, 606–609. [CrossRef]
9. Elasha, F.; Greaves, M.; Mba, D.; Fang, D. A comparative study of the effectiveness of vibration and acoustic emission in diagnosing a defective bearing in a planetary gearbox. *Appl. Acoust.* **2017**, *95*, 115–181.
10. Filippov, A.V.; Rubtsov, V.E.; Tarasov, S.Y.Y. Acoustic emission study of surface deterioration in trip contacting. *Appl. Acoust.* **2017**, *12*, 106–117.
11. Strombergsson, D.; Marklund, P.; Edin, E.; Zeman, F. Acoustic emission monitoring of mechanic-chemical surface finishing process. *Tribol. Int.* **2017**, *36*, 112–129.
12. Boaron, A.; Weingaertner, W.L. Dynamic in-process characterisation method based on acoustic emission for topographic assessment of conventional grinding wheels. *Wear* **2018**, *29*, 218–406.
13. Sadegh, H.; Mehdi, A.N.N.; Mehdi, A. Classification of acoustic emission signals generated from journal bearing at different lubrication conditions based on wavelet analysis in combination with artificial neural network and genetic algorithm. *Tribol. Int.* **2016**, *95*, 426–434. [CrossRef]
14. Kishawy, H.A.; Hegab, H.; Umer, U.; Mohany, A. Application of acoustic emissions in machining processes: Analysis and critical review. *Int. J. Adv. Manuf. Technol.* **2018**, *98*, 1391–1407. [CrossRef]
15. Badger, J.; Murphy, S.; O'Donnell, G. Acoustic emission in dressing of grinding wheels: AE intensity, dressing energy, and quantification of dressing sharpness and increase in diamond wear-flat size. *Int. J. Mach. Tools Manuf.* **2018**, *125*, 11–19. [CrossRef]
16. Douglas, R.M.; Steel, J.A.; Reuben, R.L. A study of the tribological behaviour of piston ring/cylinder liner interaction in diesel engines using acoustic emission. *Tribol. Int.* **2006**, *39*, 1634–1642. [CrossRef]
17. Asamene, K.; Sundaresan, M. Analysis of experimentally generated friction-related acoustic emission signals. *Wear* **2012**, *296*, 607–618. [CrossRef]
18. Tian, P.; Tian, Y.; Shan, L.; Meng, Y.; Zhang, X. A correlation analysis method for analysing tribological states using acoustic emission, frictional coefficient, and contact resistance signals. *Friction* **2015**, *3*, 36–46. [CrossRef]
19. Diniz, A.E.; Dornfeld, D.A. Correlating tool life, tool wear and surface roughness by monitoring acoustic emission in finish turning. *Wear* **1992**, *152*, 395–407. [CrossRef]
20. Reddy, T.S.; Reddy, C.E. Realtime monitoring of surface roughness by acoustic emissions in CNC turning. *J. Eng. Sci. Technol.* **2010**, *3*, 111–115.
21. Emel, E.; Kannatey-Asibu, E., Jr. Tool Failure Monitoring in Turning by Pattern Recognition Analysis of AE Signals. *ASME J. Eng. Ind.* **1988**, *110*, 137–145. [CrossRef]
22. Diei, E.N.; Dornfeld, D. A model of tool fracture generated acoustic emission during machining. *Trans. ASME J. Eng. Ind.* **1987**, *109*, 227–233. [CrossRef]
23. Stoica, N.A.; Petrescu, A.M.; Tudor, A.; Pedrescu, A. Tribological properties of the disc brake friction couple materials in the range of small and very small speeds. In *IOP Conference Series: Materials Science and Engineering, Proceedings of the 13th International Conference on Tribology (ROTRIB'16), Galati, Romania, 22–24 September 2016*; IOP Publishing: Galati, Romania, 2017; Volume 174. [CrossRef]
24. Matcharashvili, T.; Chelidze, T.; Zhukova, N.; Mepharidze, E. Investigation of acoustic emission accompanying stick-slip movement of rock samples at different spring stiffnesses–block system. *Tribol. Int.* **2011**, *44*, 811–819. [CrossRef]
25. Thompson, B.D.; Young, R.P.; Lockner, D.A. Observations of premonitory acoustic emission and slip nucleation during a stick-slip experiment in smooth faulted Westerly granite. *Geophys. Res. Lett.* **2005**, *32*, 1–4. [CrossRef]
26. Začal, J.; Dostál, P.; Šustr, M.; Dobrocký, D. Acoustic emission during tensile testing of composite materials. *Acta Univ. Agric. et Silvic. Mendel. Brun.* **2017**, *65*, 1309–1315. [CrossRef]
27. Chuanjun, L.; Shuangfu, S.; Yuming, W.; Weifeng, H.; Ying, L. Study on Stick-Slip Friction of Reciprocating O-RingSeals Using Acoustic Emission Techniques. *Tribol. Trans.* **2012**, *55*, 43–51.
28. Ferrer, C.; Salas, F.Ã.; Pascual, M.; Orozco, J. Discrete acoustic emission waves during stick-slip friction between steel samples. *Tribol. Int.* **2010**, *43*, 1–6. [CrossRef]
29. Martinez, E.; Picas, I.; Romeu, J.; Casellas, D. Filtering of Acoustic Emission Signals for the Accurate Identification of Fracture Mechanisms in Bending Tests. *Mater. Trans.* **2013**, *54*, 1087–1094. [CrossRef]
30. Hase, A.; Mishina, H.; Wada, M. Microscopic study on the relationship between AE signal and wear amount. *Wear* **2013**, *308*, 142–147. [CrossRef]
31. Meriaux, J.; Boinet, M.; Fouvry, S.; Lenain, J.C. Identification of fretting fatigue crack propagation mechanisms using acoustic emission. *Tribol. Int.* **2010**, *43*, 2166–2174. [CrossRef]
32. Shiotani, T. *Parameter Analysis, Acoustic Emission Testing*; Springer Nature: Berlin/Heidelberg, Germany, 2008; pp. 41–51.
33. González, E.M. Detection of Failure Mechanisms of Tool Steels by Means of Acoustic Emission Technique. Ph.D. Thesis, Escola Universitària d'Enginyeria Tècnica Industrial de Barcelona, Mechanical Engineering Department, Universitat Politèc-nica de Catalunya (UPC), 2013.

34. Sun, J.; Wood, R.J.K.; Wang, L.; Care, I.; Powrie, H.E.G. Wear monitoring of bearing steel using electrostatic and acoustic emission techniques. *Wear* **2005**, *259*, 1482–1489. [CrossRef]
35. Benabdallah, H.S.; Aguilar, D.A. Acoustic Emission and its Relationship with Friction and Wear for Sliding Contact. *Tribol. Trans.* **2008**, *51*, 738–747. [CrossRef]
36. Boness, R.J.; Hawthorne, H.M. Acoustic emission from the unlubricated sliding wear of steel and silicon nitride. *Tribol. Trans.* **1995**, *38*, 293–298. [CrossRef]
37. Zuo, L.; Zuo, D.; Zhu, Y.; Wang, H. Acoustic emission analysis for tool wear state during friction stir joining of SiCp/Al composite. *Int. J. Adv. Manuf. Technol.* **2018**, *99*, 1361–1368. [CrossRef]
38. Hanchi, J.; Klamecki, B.E. Acoustic emission monitoring of the wear process. *Wear* **1991**, *145*, 1–27. [CrossRef]
39. Eid, H.; Adams, G.G.; McGruer, N.E.; Fortini, A.; Buldyrev, S.; Srolovitz, D. A Combined Molecular Dynamics and Finite Element Analysis of Contact and Adhesion of a Rough Sphere and a Flat Surface. *Tribol. Trans.* **2011**, *54*, 920–928. [CrossRef]
40. Mulakaluri, N.; Persson, B.N.J. Adhesion between elastic solids with randomly rough surfaces: Comparison of analytical theory with molecular-dynamics simulations. *EPL* **2011**, *96*, 66003. [CrossRef]
41. Persson, B.N.J. Sliding Friction. In *Physical Principles and Applications*; Springer-Verlag: New York, NY, USA, 2000.
42. Babici, L.M.; Tudor, A.; Stoica, N.A.; Stoica, M. Acoustic emission in stick-slip phenomena of wheel-rail contact for variable velocity. In Proceedings of the 13th International Workshop on Railway Noise, Ghent, Belgium, 16–20 September 2019.
43. Nettleton, D. *Commercial Data Mining-Processing, Analysis and Modelling for Predictive Analytics Projects*; Morgan Kaufmann: Boston, MA, USA, 2014.
44. Boslaugh, S.; Watters, P.A. *Statistics in a Nutshell: A Desktop Quick Reference*; O'Reilly Media: Sebastopol, CA, USA, 2008; Chapter 7, ISBN-13 978-0596510497.
45. Zhan, W.; Fink, R.; Fang, A. Application of Statistics in Engineering Technology Programs. *Am. J. Eng. Educ.* **2010**, *1*, 65–78. [CrossRef]
46. Archard, J.F. Wear Theory and Mechanisms. In *Wear Control Handbook*; Peterson, M.B., Winer, W.O., Eds.; ASME: New York, NY, USA, 1980; pp. 35–80.
47. Bhushan, B. *Principle and Applications of Tribology*; John Wiley & Sons Inc: New York, NY, USA, 1999; pp. 344–430.
48. Chowdhury, M.A.; Khalil, M.K.; Nuruzzaman, D.M.; Rahaman, M.L. The Effect of Sliding Speed and Normal Load on Friction and Wear. *Int. J. Mech. Mechatron. Eng.* **2011**, *11*, 53–57.
49. Ozaki, S.; Matsuura, T.; Maegawa, S. Rate, state and pressure-dependent friction model based on the elastoplastic theory. *Friction* **2020**, *8*, 768–783. [CrossRef]
50. Lontin, K.; Khan, M. Interdependence of friction, wear, and noise. *Friction* **2021**, *9*, 1319–1345. [CrossRef]
51. Gourdon, D.; Israelachvili, J.N. Transitions between smooth and complex stick-slip sliding of surfaces. *Am. Phys. Soc.* **2003**, *68*, 1–10. [CrossRef] [PubMed]
52. Pavelescu, D.; Tudor, A. The sliding friction coefficient-its evolution and usefulness. *Wear* **1987**, *120*, 321–336. [CrossRef]
53. Heslot, F.; Baumberger, T.; Perrin, B. Creep, stick-slip, and dry-friction dynamics: Experiments and a heuristic model. *Am. Phys. Soc.* **1994**, *49*, 4950–4973. [CrossRef] [PubMed]
54. Caroli, C.; Nozieres, P.; Persson, B.N.J.; Tossatti, E. Dry friction as a hysteretic elastic response. In *Physics of Sliding Friction*; Springer: Dordrecht, The Netherlands, 1995; pp. 27–49.